Iranian Journal of Materials Forming 11 (2) (2024) 30-45

Online ISSN: 2383-0042

Iranian Journal of Materials Forming

Journal Homepage: http://ijmf.shirazu.ac.ir

Research Article

Constitutive Modeling and Microstructural Evolution of Hot Deformed Ti-6Al-4V Alloy Starting with Initial Fully Lamellar Microstructure

R. Gostariani[1*], G. Vaez[2], M. Ansaripour[2] and A. Babanejad[1]

[1] Reactor and Nuclear Safety Research School, Nuclear Science and Technology Research Institute, P.O. Box: 14395-836, Tehran, Iran
[2] Atomic Energy Organization of Iran, P.O. Box: 14155-1339, Tehran, Iran

ARTICLE INFO

Article history:

Received 16 April 2024
Reviewed 22 June 2024
Revised 3 July 2024
Accepted 30 July 2024

Keywords:

Ti-6Al-4V alloy
Hot deformation
Lamellar microstructure
Dynamic recrystallization
Constitutive modeling

Please cite this article as:

Gostariani, R., Vaez, G., Ansaripour, M., & Babanejad, A. (2024). Constitutive modeling and microstructural evolution of hot deformed Ti-6Al-4V alloy starting with initial fully lamellar microstructur. *Iranian Journal of Materials Forming*, *11*(2), 30-45. https://doi.org/10.22099/IJMF.2024. 49974.1292

ABSTRACT

Ti–6Al–4V alloy has gained widespread popularity due to its extensive applications, including nuclear and aircraft structural components, machine parts, and notably medical equipment parts. Gaining a comprehensive understanding of the material's deformation behavior and microstructure evolution during the hot working process is crucial in order to attain the desired dimensions and the final mechanical properties of a product. In this study, the hot deformation behavior of the fully lamellar Ti-6Al-4V alloy was investigated using the hot compressive test at different temperatures of 700-1050 ˚C and strain rates of 0.001-1 s^{-1}. The deformation stress, strain rate, and temperature were correlated using Arrhenius constitutive equations in α + β and β-phases. Finally, the activation energy values were calculated at almost 630 kJ/mol and 293 kJ/mol in α + β and β-phases, respectively. Based on true stress-strain curves, dynamic recrystallization was the dominant hot deformation mechanism at strain rates of 0.1 s^{-1} or lower. On the other hand, dynamic recovery occurred at a low temperature of 700 ˚C, and high temperatures of 1000-1050 ˚C with high strain rates of 1 s^{-1}. The dynamic strain aging was visible as the serrated effects on deformation curves. The hot deformed microstructures of Ti-6Al-4V alloy were changed through geometric dynamic recrystallization, lamellar kinking and fragmentation, and globularization. Microstructural evolution at low temperatures immediately initiated after peak stress with dynamic recrystallization and lamellar kinking. At high temperatures of 850-900 ˚C, globularization was combined with other softening mechanisms, and the lamellar microstructure was changed to equiaxed grains.

1. Introduction

Titanium alloys are commonly used in various aerospace, nuclear, energy, and defense industries due to their unique properties, such as high specific strength, high corrosion resistance, and high thermal stability [1]. In the nuclear industry, titanium alloys are used in the structural components of the first loop of pressurized nuclear reactors due to their low neutron activation and high mechanical properties [2]. Resistance to fatigue and corrosion, combined with high strength, has led to the use of titanium alloys in the construction of high-speed centrifuges [3]. Russian submarines' low-weight and high-strength hulls in the

* Corresponding author
E-mail address: rgostariani@aeoi.org (R. Gostariani)
https://doi.org/10.22099/IJMF.2024.49974.1292

1970s were constructed of titanium alloy sheets [3]. The Ti-6Al-4V alloy comprised approximately half of all titanium alloys used in various industries. The high mechanical properties and suitable intrinsic workability provide the ability to manufacture the complex parts of Ti-6Al-4V alloy [4]. The non-toxic properties and compatibility of this alloy have positioned Ti-6Al-4V as a favored choice for dental and surgical implants [5]. The dual α+β-phase Ti-6Al-4V has corrosion and fatigue resistance properties and is utilized in high-intensity proton accelerator facilities [6, 7]. The Ti-6Al-4V alloy has poor workability at room temperature; therefore, the deformation of this alloy is performed at high temperatures [8]. On the other hand, this alloy is sensitive to the conditions of the manufacturing process. In addition, the hot deformation has a good impact on its final microstructure [4]. The initial microstructure and its evolution during hot deformation play a significant role in determining the ultimate properties of Ti-6Al-4V, including fatigue, tensile strength, and failure mechanisms [9-11]. Evidently, the lamellar microstructure exhibits high work hardening behavior and strength. Conversely, the formation of globular and equiaxed microstructures enhances ductility [10]. Although there are uncertainties regarding the impact of microstructure on fatigue behavior, it appears that the development of an equiaxed microstructure leads to improved fatigue properties [11]. The constitutive equation is one of the most accurate and well-known methods to estimate the flow stress of alloys as a function of temperature and strain rate in the hot deformation process [12]. In recent years, various research has been conducted on the evaluation of the hot deformation behavior of Ti-6Al-4V alloys. The representative parameters of the hot deformation behavior of this alloy change with the initial microstructure. Table 1 lists the results of the evaluation of its hot deformation behavior [13-23].

Table 1. Information about activation energy and deformed microstructure in literature review

Alloy	Initial microstructure	Hot deformation condition	Obtained activation energy (kJ/mol)	Hot deformed microstructure	Hot deformation mechanism	Ref.
Ti–6Al–4V	Equiaxed and elongated α + intergranular β	750–950 °C 0.01–10 s^{-1}	550.9	Globularized microstructure (T > 900 °C) Serrated α grains, rotated and kinked α laths (T= 780 °C)	Dynamic globularization Dynamic recovery (DRV)	[13]
	Fine acicular α	850–1050 °C 0.01–10 s^{-1}	672.6–525.3 (strain of 0.1–0.9)	Martensitic $\acute{\alpha}$ microstructure (T > 950 °C) Primary equiaxed and elongated α–phase + needle-like β–phase (T< 850 °C)	DRV Dynamic recrystallization (DRX)	[14]
	Lamellar	750–950 °C 0.01–10 s^{-1}	522	Globularized microstructure (T= 900 °C) and kinked lamellar (T= 750 °C)	–	[15]
	–	880–950 °C 1–50 s^{-1}	501	α-phase grains with a small amount of intergranular β–phase	–	[16]
	–	800-1150 °C 0.001–1 s^{-1}	530 (α+β–phase) 379 (β–phase)	Globularized α (T= 900–950 °C) β transformed grains	DRX	[17]
	Equiaxed primary α-phase and retained β	800–1050 °C 0.001–1 s^{-1}	535 (800–900 °C) 350 (950–1050°C)	–	–	[18]

Table 1. (*continued*)

Alloy	Initial microstructure	Hot deformation condition	Obtained activation energy (kJ/mol)	Hot deformed microstructure	Hot deformation mechanism	Ref.
Ti−6Al−4V	Acicular	850–1050 °C 0.001–5 s^{-1}	425.5	Deformed microstructure (T< 900 °C)	DRV	[19]
				Recrystallized grains (T= 950 °C)	DRX	
	Lamellar	750–950 °C 0.001–10 s^{-1}	510 (Strain of 0.1)	Globularized α (T= 750-950 °C, low strain rate)	DRX	[20]
				Kinked microstructure (T= 750–950 °C, high strain rate)	kinking (or buckling) of α-laths	
				Bimodal microstructure (T > 850 °C)		
	Equiaxed		580 (Strain of 0.1)	Primary α–phase is partitioned into Primary α and β (T< Transus Temperature)		
	-	850–950 °C 0.001–1 s^{-1}	689.3	–	DRX DRV	[21]
	Thick lamellar	Hot Tensile 850–900 °C 0.0005–0.005 s^{-1}	420.3	Elongated and bent α (T= 850 °C)	DRX	[22]
				Globularized α (T= 900 °C)	Dynamic globularization	
	Coarse acicular α+β	800–1050 °C 0.001–10 s^{-1}	620.6	Elongated α in transformed β (T= 800–850 °C)	DRX DRV	[23]
				Equiaxed α–β (T > 950 °C)	Dynamic globularization	

The present study addresses the existing research gap by investigating the microstructural evolution and globularization occurrence in the Ti-6Al-4V alloy during straining at the recrystallization temperature. The novelty of this research lies in its focus on understanding the unique behavior of the alloy under these specific conditions, relatively underexplored in previous studies. For this purpose, the hot compression test on the initial fully lamellar microstructure in the Ti-6Al-4V alloy is performed at different temperatures and strain rates. This evaluation is executed by developing a constitutive equation and observing the deformed microstructure.

2. Experimental Procedure

The cylindrical hot compression test samples of the Ti-6Al-4V were prepared with a diameter of 9 mm and a height of 13 mm. The hot compression tests were conducted on the ZwickRoell 250 testing machine in a temperature range of 700-1050 °C with strain rates of 0.001 to 1 s^{-1}. A mica sheet, used as the heat-resistant lubricant, was placed between anvils to reduce friction in the test. After the test sample was isothermally heated for 10 minutes to reach the test temperature, the compressive force was applied up to strain 0.9 and then the sample was rapidly cooled in water. The true stress-strain curves were generated by correcting for strain rate changes during the compression test conducted at a constant ram speed. Furthermore, the

curves were adjusted to account for the elimination of friction and adiabatic effects. The upper-bound theory developed by Ebrahimi et al. [24] was utilized to eliminate the effect of friction from the true stress-strain data. Detailed instructions on how to remove adiabatic effects and strain rate changes were provided in a previous study [25].

The phase transformation temperatures were identified using a Baehr DIL 805 A/D Dilatometer. Dilatational testing was conducted on a test specimen size of 4 mm in diameter and 10 mm in height under a vacuum of 5×10^{-4} mbar.

Optical and scanning electron microscopes were employed to examine the microstructural evolution in the study. To facilitate this investigation, the hot deformed samples were cut in the direction of compression. The resulting cross-sections underwent a series of preparation steps, including polishing, followed by etching in a solution composed of 85 ml of distilled water, 10 ml of HNO_3, and 5 ml of HF.

The Arrhenius constitutive equation presented by Sellars and Tegart et al. [26] is widely used to relate flow stress, temperature, and strain rate in the hot deformation process. This kinetic modeling is proposed as the following equations [26]:

$$\begin{cases} \dot{\varepsilon} = A_1 \sigma^{n_1} \exp\left(-Q/RT\right) & \text{low stress level} \\ \dot{\varepsilon} = A_2 \exp(\beta\sigma) \exp\left(-Q/RT\right) & \text{high stress level} \\ \dot{\varepsilon} = A\,[\sin h(\alpha\sigma)]^n \exp\left(-Q/RT\right) & \text{all stress levels} \end{cases} \quad (1)$$

In the above equations, the symbols have the following meanings:

σ (MPa) and $\dot{\varepsilon}$ (s^{-1}) represent the flow stress and strain rate, respectively. R is the universal gas constant and is equal to 8.314 (J/mol K). T (K) represents the absolute temperature. Q represents the activation energy of deformation. A (s^{-1}), A_1 (s^{-1}), A_2 (s^{-1}), β (MPa^{-1}), and α (MPa^{-1}) = β/n_1 are material constants. Additionally, n and n_1 refer to the stress exponents.

After taking the natural logarithm of the two sides of constitutive equations, the material constants of n_1, β, and n were calculated from the average slope of ln$\dot{\varepsilon}$- lnσ, ln$\dot{\varepsilon}$- σ, and ln$\dot{\varepsilon}$- ln $\sin h(\alpha\sigma)$. In these equations, the peak stress of the experimental data was used.

To calculate the activation energy value, the partial differential was taken from the natural logarithm of the constitutive equation at all stress levels and presented in the following relation:

$$Q = R\left[\partial ln\dot{\varepsilon}/\partial ln[\sinh(\alpha\sigma)]\right]_T \cdot \left[\partial ln[\sinh(\alpha\sigma)]/\partial(1/T)\right]_{\dot{\varepsilon}} \quad (2)$$

The activation energy and the Zener-Hollomon parameter (Z) are related by the following equation [27]:

$$Z = \dot{\varepsilon}\, exp(\tfrac{Q}{RT}) \quad (3)$$

From the combination of Eqs. (1) and (3) and taking the natural logarithm, the Zener-Hollman equation is obtained as follows:

$$lnZ = ln\, A + n\, ln[\, sinh(\, \alpha\sigma)] \quad (4)$$

The value of the stress exponent (n) was determined using the slope of the linear fitting plot of ln Z- ln $\sin h(\alpha\sigma)$. Finally, the flow stress is estimated using the following equation:

$$\sigma = \frac{1}{\alpha} ln\left\{\left(\frac{Z}{A}\right)^{1/n} + \left[\left(\frac{Z}{A}\right)^{2/n} + 1\right]^{1/2}\right\} \quad (5)$$

3. Results and Discussion

3.1. Phase transformation temperatures

The phase transformation temperatures of the Ti-6Al-4V alloy are shown in Fig. 1. The α+β phase region appeared at a temperature of 882 ˚C. The β transus temperature ($\alpha + \beta \rightarrow \beta$) is measured at 965 ˚C.

3.2. Initial microstructure

Fig. 2 shows the as-received microstructure of Ti-6Al-4V alloy. It consists of α grains with β grain boundaries. This coarse weave-basket microstructure appeared from slow cooling from the β-phase region. The average width of the α layers is less than 3 μm.

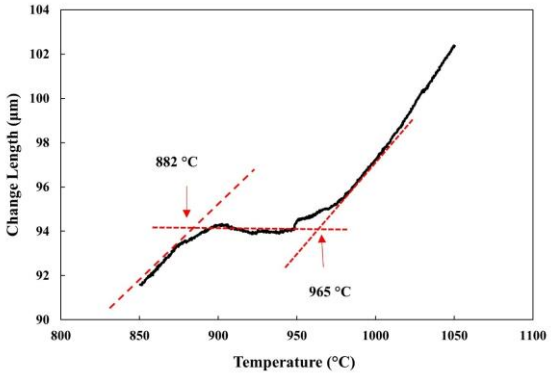

Fig. 1. Determining phase transformation temperatures using dilatometric test.

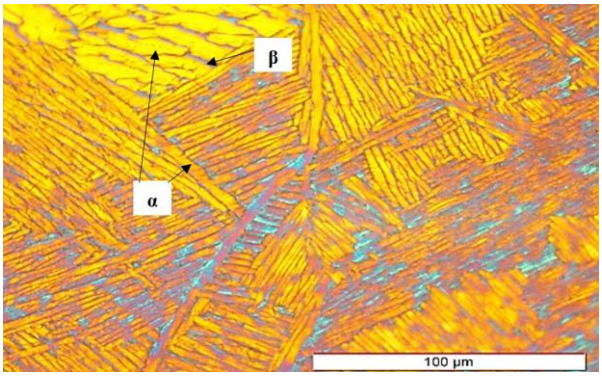

Fig. 2. The as-received microstructure of Ti-6Al-4V alloy.

3.3. Hot compressive behavior

The hot compressive true stress-true strain curves of Ti-6Al-4V alloy at different temperatures (700-1050 ˚C) and strain rates (0.001-1 s^{-1}) are shown in Fig. 3. The hot compression behavior of the Ti-6Al-4V alloy is similar to other materials and its hot compressive flow stress decreases by increasing the temperature and decreasing the strain rate. The shape of hot deformed stress-strain curves indicated the type of metallurgical phenomena occurrence such as work hardening and work softening (dynamic recovery and recrystallization). At the beginning of straining, the hot compressive stress increases up to the peak point due to the work hardening mechanism with the increasing dislocation density and interaction. The softening mechanism is activated after the peak point. Dynamic recrystallization occurrence reduces the flow stress until the steady-state region. On the other hand, dynamic recovery led to immediately going from the flow stress to the steady-state region without decreasing from the peak point. The compressive stress does not change through straining in the steady-state region [28].

As shown in Fig. 3, dynamic recrystallization is considered as the dominant mechanism of hot deformation at all temperatures (700-1050 ˚C). In addition, the strain rates that range from 0.001 to 0.1 s^{-1} decrease the compressive stress to the steady-state region. As the strain rate increases in the range of 0.001 to 0.1 s^{-1}, the distance between the strain at the peak point and the strain at the beginning of the steady-state region decreases. In other words, the increasing rate of straining led to an increase in the driving force to accelerate the speed of the softening mechanism. At a high strain rate of 1 s^{-1} and a low temperature of 700 ˚C and high temperatures in β-phase 1000-1050 ˚C (Fig. 3(e)), the dominant mechanism of hot deformation of the Ti-6Al-4V alloy is recovery. At intermediate temperatures in the α-phase (750-950 ˚C), the dynamic recrystallization at a strain rate of 1 s^{-1} reduces the flow compressive stress up to the steady-state region.

The serrated effects are observed in the plastic region of the hot deformation curve of alloy Ti-6Al-4V in the temperature range of 700-1050 ˚C and low strain rates of 0.001- 0.01 s^{-1}. These results are shown in Fig. 4 for the temperature range of 700-950 ˚C and strain rates 0.001-0.01 s^{-1}. Fig. 3(b) and 3(d) also show the serrated effects for the higher temperatures of 950-1050 ˚C. As can be seen, the fluctuation intensity is increased from 700 ˚C to 800 ˚C and then noticeably decreased at a temperature range of 850-1050 ˚C. On the other hand, the maximum intensity of fluctuation is at a temperature range of 800-900 ˚C. These serrated effects are attributed to dynamic strain aging (DSA). DSA is a result of the interaction between solute atoms with mobile dislocations. The solute atoms, including alloying elements and impurities, diffuse to the edge dislocations core and create the Cottrell atmosphere [29, 30].

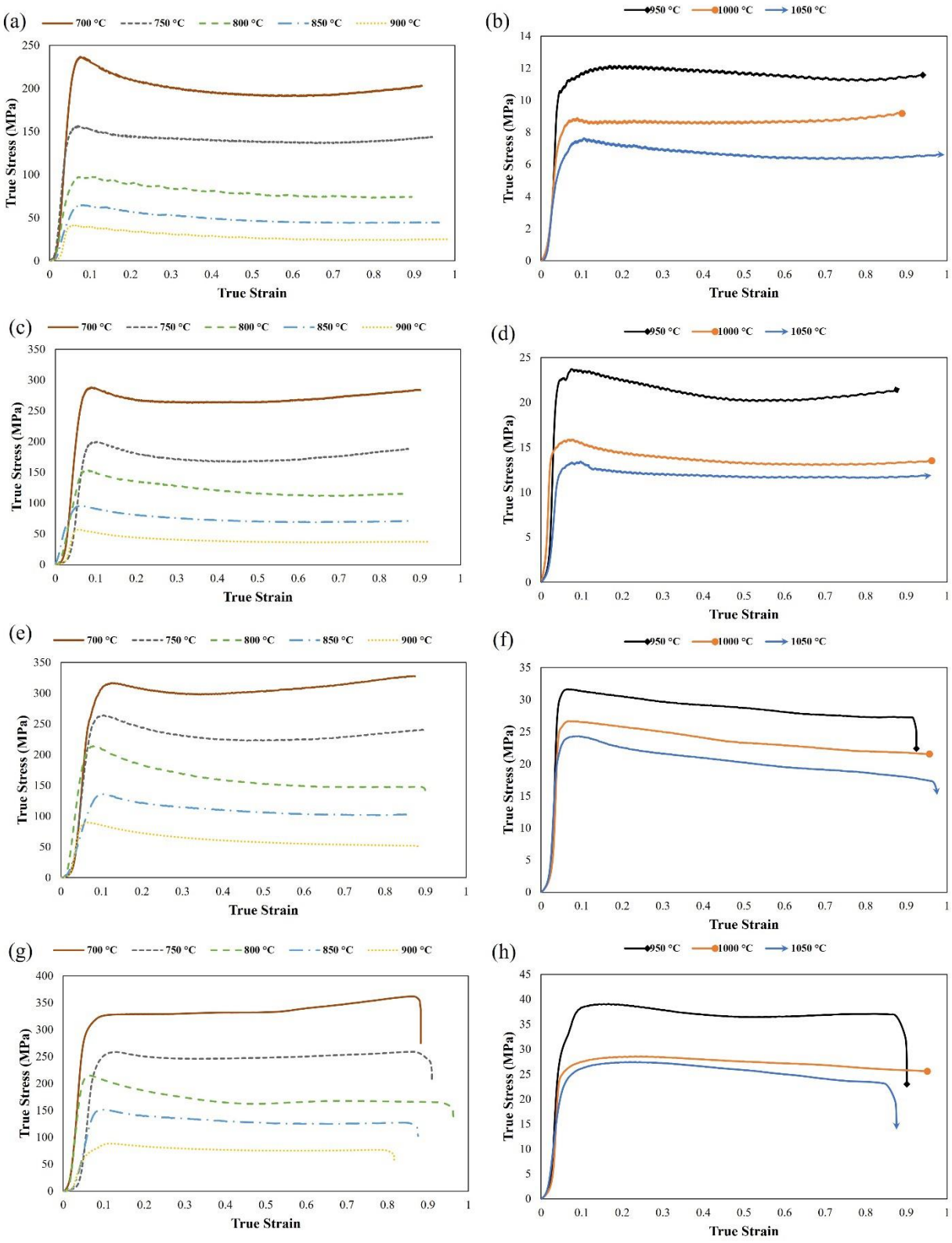

Fig. 3. Hot compressive stress of Ti-6Al-4V alloy at various temperatures of 700-1050 ˚C and strain rates of (a, b) 0.001 s^{-1}, (c, d) 0.01 s^{-1}, (e, f) 0.1 s^{-1}, and (g, h) 1 s^{-1}.

This phenomenon acts as an obstacle against the dislocation motion. The unpinning dislocation is accompanied by an increase in deformation stress and a decrease after crossing the obstacles. These solute atoms diffuse again toward the dislocations and this repeated cycle, including dislocation pinning and dislocation unpinning, led to generating the stress fluctuation in deformation curves. Based on the observation in Fig. 3 and Fig. 4, the dynamic strain aging is sensitive to strain rate and temperature. The serrated effects are less at low temperatures of 700-750 ˚C and very high temperatures of 950-1050 ˚C. The low diffusion rate of solute atoms at 700 ˚C and the high rate of the climb and cross sliding the dislocation at high temperatures of 950-1050 ˚C led to a decrease in the serrations. On the other hand, the depth of the serrations is increased at temperatures from 800 ˚C to 900 ˚C. As can be seen in Fig. 4(a-d), the fluctuations decrease with increasing strain rates so that no traces of these serrations are observed in the strain rates of 0.1 s^{-1} to 1 s^{-1} (Fig. 3(f, h)). By increasing the strain rate, the diffusion rate of solute atoms to the dislocations core is reduced.

Fig. 4(c) and Fig. 4(d) show a comparison between the stress-strain curve at two temperatures of 700 ˚C and 850 ˚C at a constant strain rate of 0.01. The initial strains of stable region at temperatures of 700 ˚C and 900 ˚C are 0.3 and 0.5, respectively. At a low temperature of 700 ˚C, the amount of recrystallization strain is low until it reaches the stable region, leading it to enter this region with a 10% drop from the peak stress. With the simultaneous occurrence of recrystallization and globularization, the amount of stress reduction from the peak point to the stable stress is more than 30%. Additionally, the strain interval from the peak point to the steady state point is large. The globularization process involves shearing the lamellar structure of the α phase under critical stress, leading to the formation of interfaces accompanied by dislocation generation. This process facilitates the creation of globular grains as grain boundaries migrate through diffusion [31]. Additionally, during straining, the formation of the β phase within the α phase contributes to further stress reduction, eventually reaching a stable region.

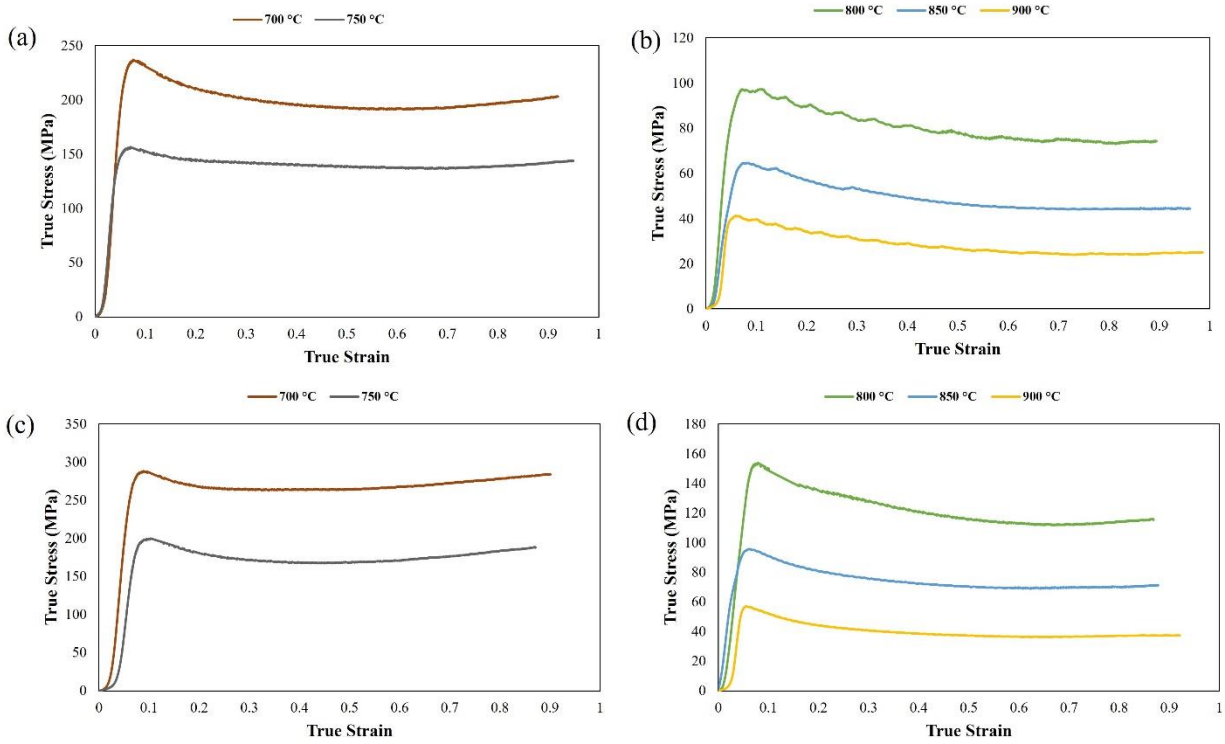

Fig. 4. Display serrated effects on true stress-true strain curves of Ti-6Al-4V alloy at various temperatures of 700-950 ˚C and strain rates of (a, b) 0.001 s^{-1}, and (c, d) 0.01 s^{-1}.

3.4. Arrhenius constitutive modeling

Arrhenius constitutive equation is commonly developed to predict deformation stress changes with strain rate and temperature based on Eq. (1). For this purpose, it is necessary to directly determine the material constant from the experimental compression data. Therefore, the Ti-6Al-4V constants of n_1, β, n, and Q, were calculated using the average slope plot values of $ln\dot{\varepsilon}$- $ln\sigma$, $ln\dot{\varepsilon}$- σ, *and* $ln\dot{\varepsilon}$- $ln\ sinh(\alpha\sigma)$, $ln\ sinh(\alpha\sigma)$-$1000/T$, respectively. The plots shown in Fig. 5 are depicted using the peak stress of the hot compression test data in two temperature ranges of 700-900 ˚C (α-phase) and 950-1050 ˚C (β-phase). Fig. 5(a) illustrates the variations in peak stress as a function of temperature at different strain rates. The values of n_1 are obtained at 10.34 and 4.97 for temperatures ranges of 700-900 ˚C and 950-1050 ˚C, respectively (Fig. 5(b)). Based on Fig. 5(c), the values of β at two temperature ranges were measured at 0.0713 MPa^{-1} (700-900 ˚C) and 0.28 MPa^{-1} (950-1050 ˚C). The values of α (in which $\alpha=\beta/n_1$) are calculated at about 0.007 MPa^{-1} for 700-900 ˚C and 0.057 MPa^{-1} for 950-1050 ˚C. By determining the value of α and the linear fitting lines in Fig. 5(d-e) and Fig. 5(f-g), the initial values of n (6.97 for 700-900 ˚C, 3.72 for 950-1050 ˚C) and Q (670 kJ/mol for 700-900 ˚C, 293 kJ/mol for 950-1050 ˚C) are obtained.

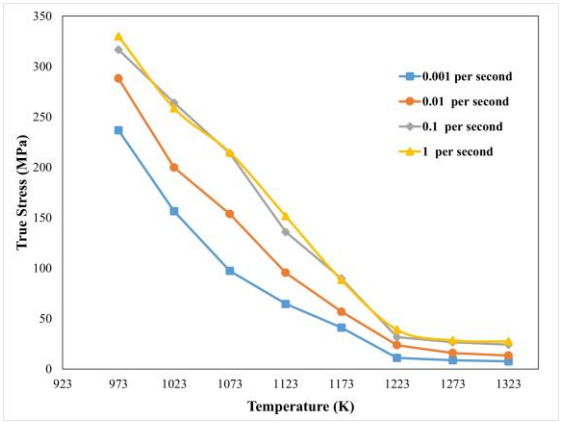

(a)

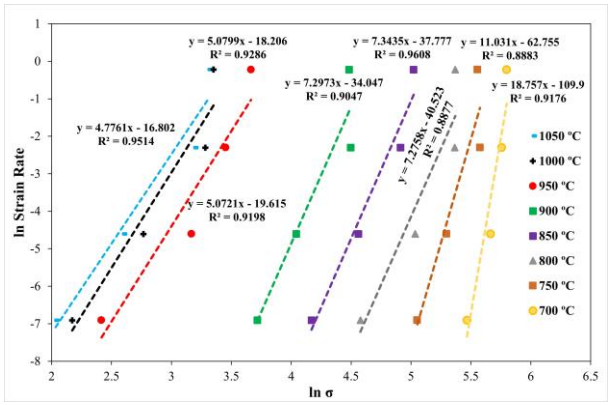

(b)

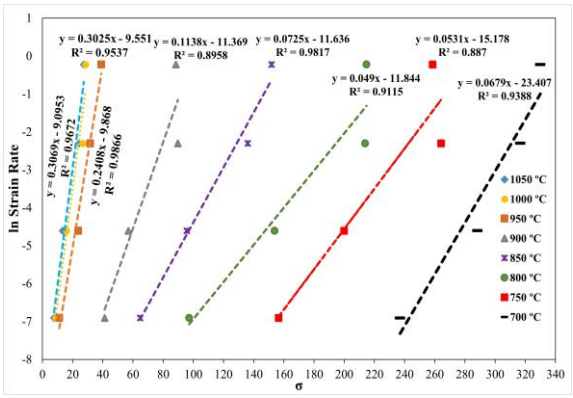

(c)

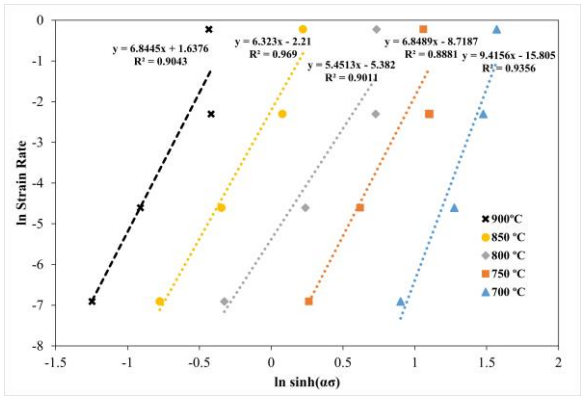

(d)

Fig. 5. Relation between peak stress vs strain rate and temperature for determining the constitutive parameters by plotting (a) σ-T (b) ln ε̇-ln σ, (c) ln ε̇- σ, (d) ln ε̇-ln sinh(ασ) for 700-900 ˚C, (e) ln ε̇-ln sinh(ασ) for 950-1050 ˚C, (f) ln sinh(ασ)-1000/T for 700-900 ˚C, and (g) ln sinh(ασ)-1000/T for 950-1050 ˚C.

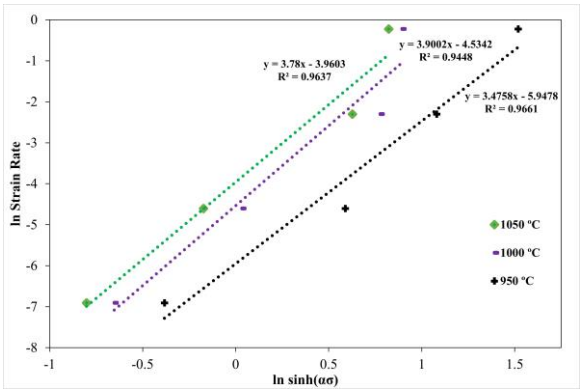

(e)

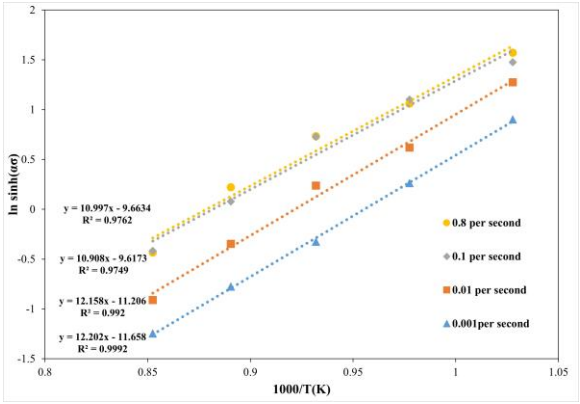

(f)

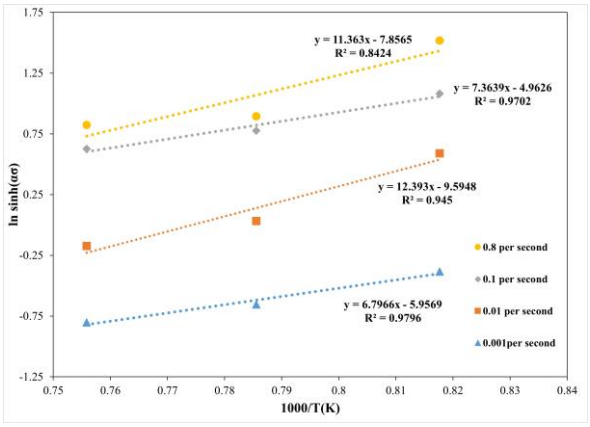

(g)

Fig. 5. (*continued*).

The values of *n* and *A* are precisely determined from the slope and the intercept of the linear plot of *ln Z-ln* $sinh(\alpha\sigma)$, respectively in Fig. 6. The accurate values of *n*, *A* and *Q* are calculated about 6.57, 5.93×10^{28} s^{-1}, 630 kJ/mol and 3.7, 9.9×10^{9} s^{-1}, 291 kJ/mol for 700-900 ˚C and 950-1050 ˚C, respectively. Finally, the constitutive equations of Ti-6Al-4V for these two temperature ranges of 700-900 ˚C and 950-1050 ˚C are presented as follows:

$$Z = \dot{\varepsilon}\ exp\ (\frac{630\times10^3}{RT}) = 5.93\times10^{28}\times(sinh(0.007\times\sigma_p)^{6.57} \quad (700\text{ -}900\ ^\circ C) \tag{6}$$

$$Z = \dot{\varepsilon}\quad exp\quad (\frac{291\times10^3}{RT}) = 9.9\times10^{9}\times(sinh(0.057\times\sigma_p)^{3.7} \quad (950\text{ -}1050\ ^\circ C) \tag{7}$$

By determining the Zener-Hollomon parameter (*Z*), the peak stress of Ti-6Al-4V was estimated using Eq. (5). Fig. 7 shows the correlation coefficient of both the experimental data and the calculated data by using the constitutive equations. The slopes of the best-fitting lines show the highest least squared error (R^2> 0.93). Therefore, it indicated that the constitutive equations accurately predict the peak stress at different temperatures and strain rates.

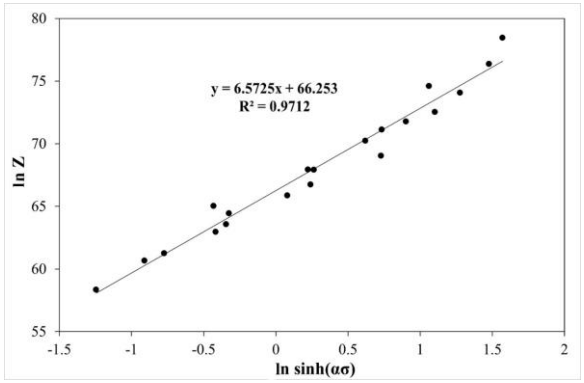

(a)

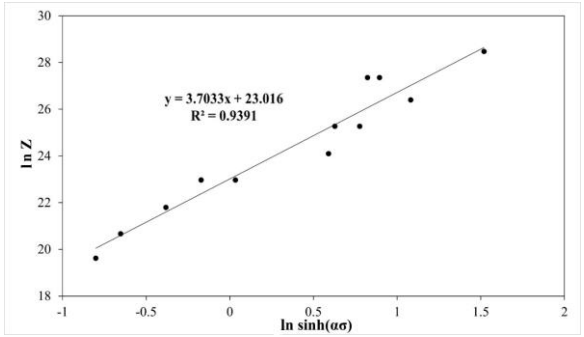

(b)

Fig. 6. The plot of ln Z- ln sin h(ασ) for determining n and A: (a) 700-900 ˚C, (b) 950-1050 ˚C.

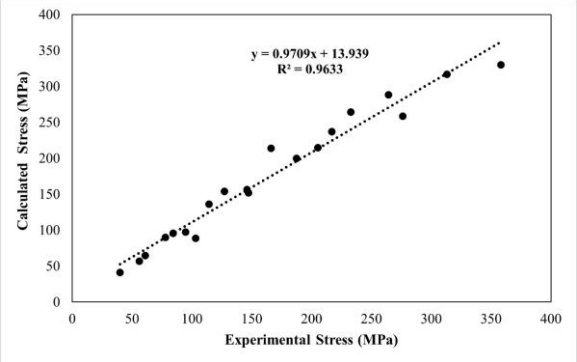

(a)

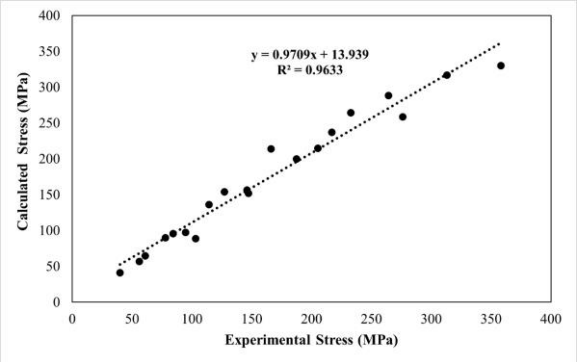

(b)

Fig. 7. Comparison between experimental and calculated peak stresses of Ti-6Al-4V; (a) 700-900 ˚C, (b) 950-1050 ˚C.

Activation energy indicates the barrier energy in atomistic mechanisms in hot deformation, which is known as an indicator of interpreting the softening mechanism in the hot deformation of materials. When the activation energy of hot working is close to the activation energy for self-diffusion, the dynamic recovery including dislocation slip and dislocation climb is the softening mechanism in hot deformation. On the other hand, the significant difference in the values of hot working and self-diffusion energies represents the occurrence of dynamic recrystallization (nucleation and growth, grain boundary migration) during hot deformation [32]. In the present study, the obtained activation energies of 630 kJ/mol in α-phase region and 291 kJ/mol in β-phase region for lamellar Ti-6Al-4V are much higher than self-diffusion activation energies of α-Ti (~151 kJ/mol [20]-242 kJ/mol [33]) and β-Ti (~97 kJ/mol [33]-153 kJ/mol [34]), respectively. The higher activation energies of α-phase with HCP compared to β-phase with BCC are attributed to the difference in the crystal lattice and more slip systems in the BCC [17].

3.5. Hot deformed microstructure

Fig. 8 and Fig. 9 show the microstructural evolution of the lamellar Ti-6Al-4V alloy after going through the hot deformation test at various temperatures and strain rates. As can be seen in Fig. 9, the microstructures are completely transformed to β-phase during the hot compression test at 950 -1050 ˚C and then converted to an α prime (martensite) phase by being rapidly cooled in water.

Dynamic recrystallization and globularization led to a change in the initial microstructure through hot deformation under the β transus temperature (Fig. 8). Hot deformation of the lamellar Ti-6Al-4V alloy at low temperatures in the range of 700- 800 ˚C leads to bending the α lamellar and the kinked microstructures being formed (shown by the arrows in Fig. 8(b, e). The lamellar rotation and kinked microstructure formation are the dynamic softening mechanism, immediately occurring after peak stress. Several nuclei were observed in grain boundaries of deformed microstructure at 750 ˚C and 0.001 s^{-1} (Fig. 8(c)). These nuclei were surrounded by two layers. The applied compression force from the deformation of the two layers has prevented nuclei growth. Since the conversion of α to β-phase due to dynamic transformation has been reported [35, 36], it seems that the nuclei are formed in the β-phase.

The globularization of the grains in microstructure starts at a temperature of 850 ˚C and a low strain rate of 0.001 s^{-1}. The geometric dynamic recrystallization (GDR) mechanism is the triggering force of grain globularization [37]. Fig. 10 and Fig. 8(i, j) show the globularized microstructure at 900˚C. The entire microstructure at a strain rate of 0.001 s^{-1} consists of equiaxed grains. As the strain rate increases, the globularization of the microstructure decreases. Therefore, at the strain rate of 1 s^{-1}, a high fraction of the microstructure remains in a lamellar form. On the other hand, Ti_3Al intermetallic precipitations formed during the initial cooling of the alloy in the furnace can be observed in the SEM micrograph.

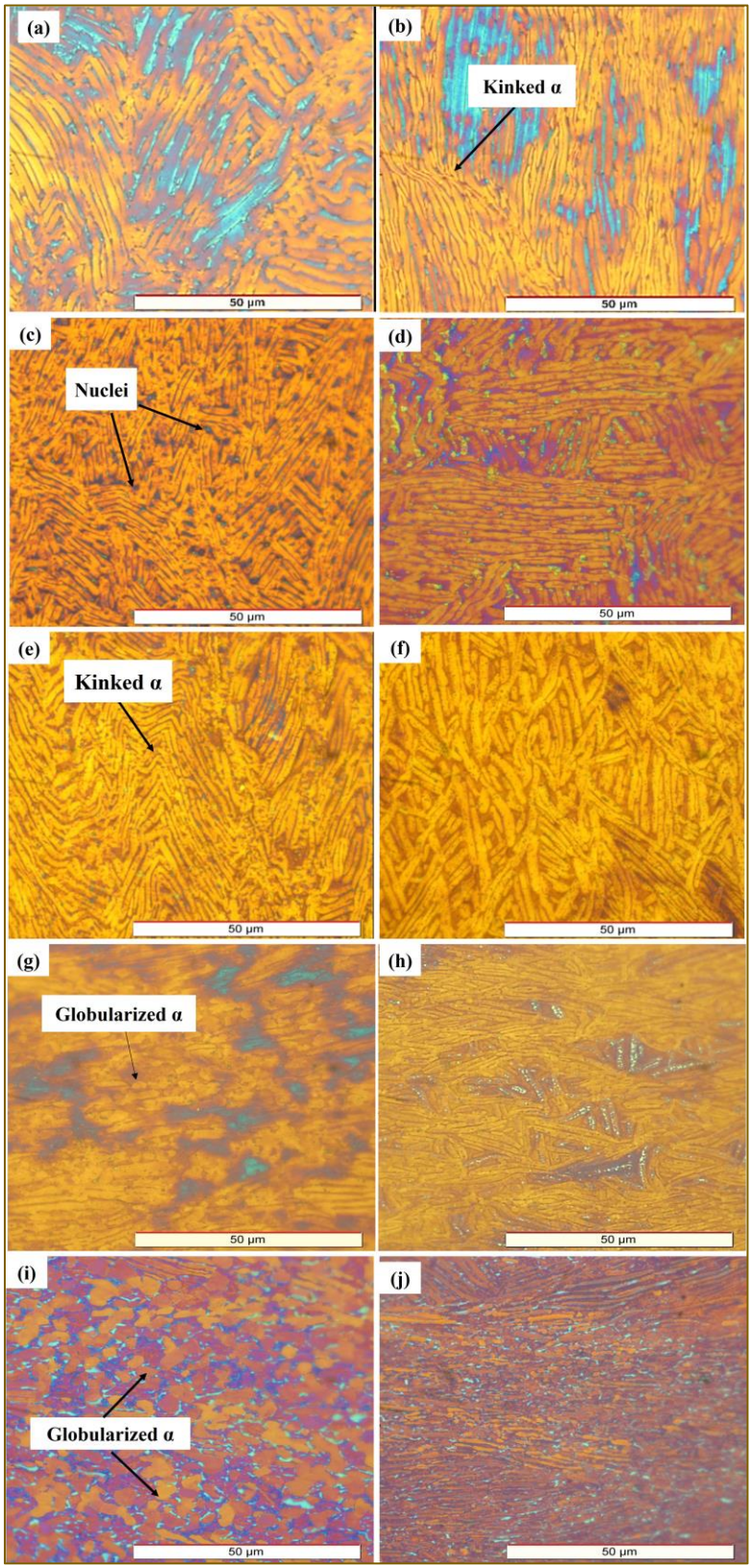

Fig. 8. The hot deformed microstructure of lamellar Ti-6Al-4V at various temperatures and strain rates of (a) 700 ˚C, 0.001 s^{-1}, (b) 700 ˚C, 0.1 s^{-1}, (c) 750 ˚C, 0.001 s^{-1}, (d) 750 ˚C, 0.1 s^{-1}, (e) 800 ˚C, 0.001 s^{-1}, (f) 800 ˚C, 0.1 s^{-1}, (g) 850 ˚C, 0.001 s^{-1}, (h) 850 ˚C, 0.1 s^{-1}, (i) 900 ˚C, 0.001 s^{-1}, (j) 900 ˚C, 0.1 s^{-1}.

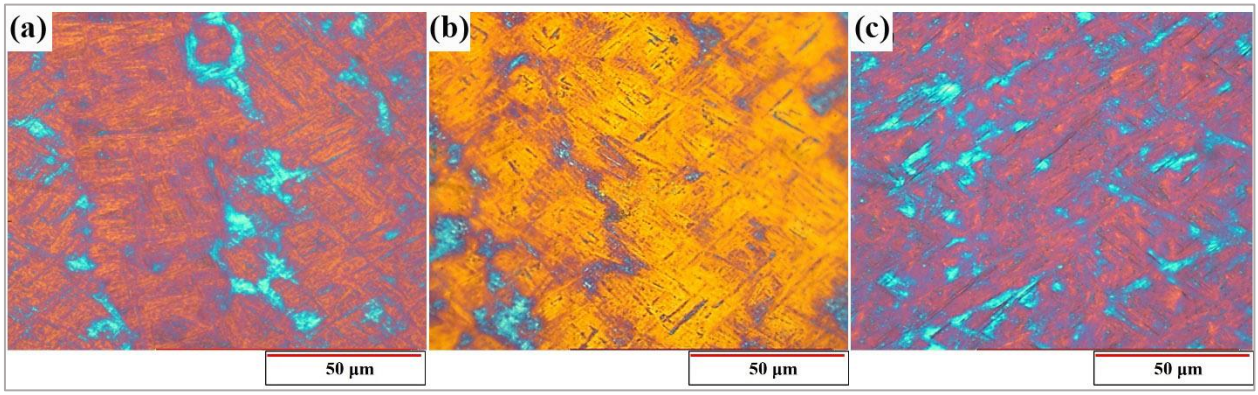

Fig. 9. The hot deformed microstructure of Ti-6Al-4V at the strain rate of 0.1 s^{-1} and various temperatures of (a) 950 ˚C, (b) 1000 ˚C, and (c) 1050 ˚C.

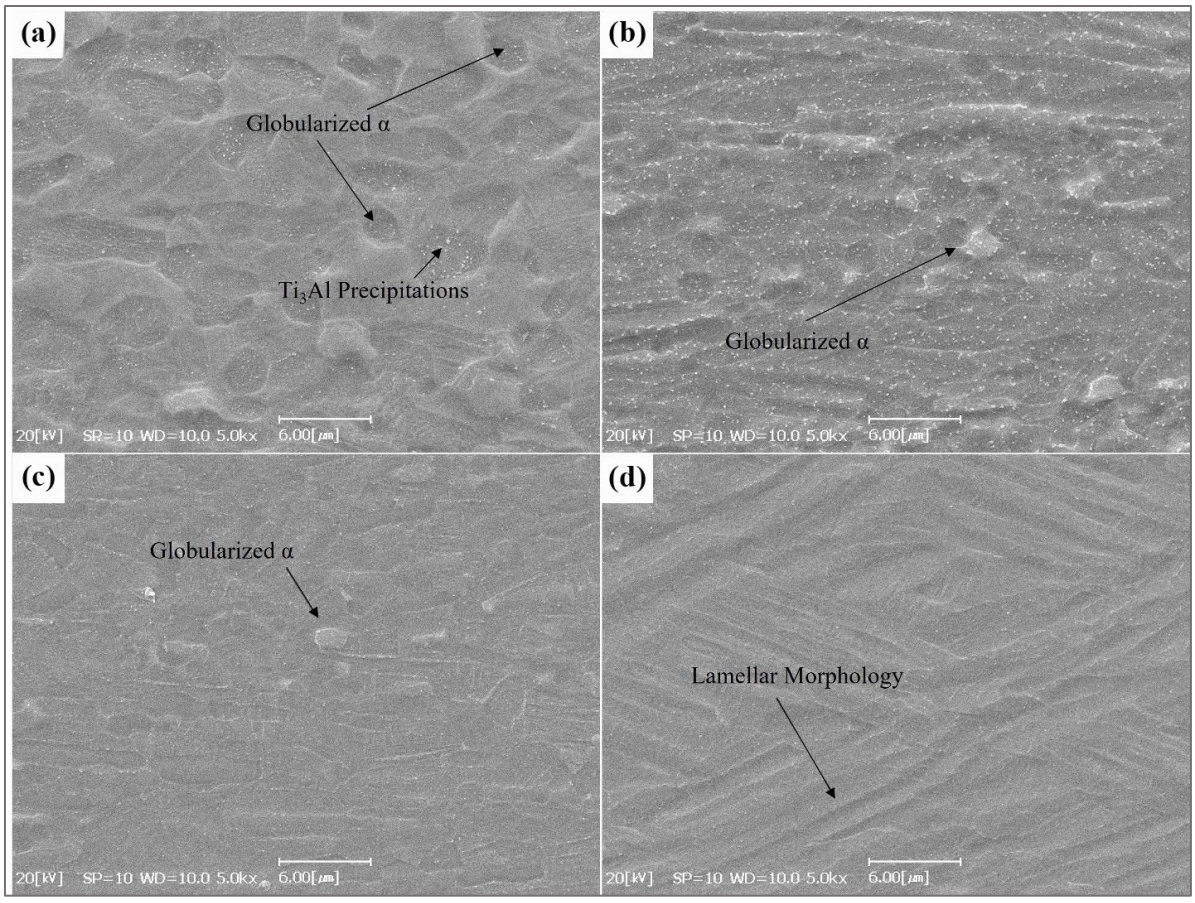

Fig. 10. The hot deformed microstructure of Ti-6Al-4V at temperature of 900 ˚C and various strain rates of (a) 0.001 s^{-1}, (b) 0.01 s^{-1}, (c) 0.1 s^{-1}, and (d) 1 s^{-1}.

Fig. 11 demonstrates how a lamellar microstructure is transformed into a globularized microstructure through the hot deformation of Ti-6Al-4V alloy. For this purpose, the hot deformed microstructure at 850 ˚C and strain rate of 0.01 s^{-1} is shown in Fig. 11 at different strains of 0.1, 0.3, and 0.5. As can be seen in Fig. 11(a), the thickness of lamellar grains (perpendicular to pressure direction) is decreased through the hot deformation, and the angular lamellar grains against the pressure direction are kinked at the initial strain of 0.1. The effects of strain localization are developed in a small fraction of lamellar grains and thinning has occurred in some lamellar grains. As the result of dynamic transformation through the high-

temperature deformation, it seems that the α-phase has converted into the β-phase in grain boundaries. This process is controlled by the rate of β-phase diffusion into the α-phase [38]. This phase transformation decreased the grain boundary strength and therefore the fragmentation of the lamellar grains is accelerated. With an increase in the strain to 0.3, the broken lamellar grains increased significantly and can be seen as islands in Fig. 11(b). In addition, the fraction of globularized grains increased. By increasing the strain up to 0.5, almost many lamellars have turned into globularized grains, which have not been completely separated from the lamellar grains and have not become equiaxed. The lamellar microstructure is replaced by the globularized microstructure with multiple and simultaneous mechanisms of dynamic recrystallization, boundary splitting, shearing mechanism, and termination migration [37].

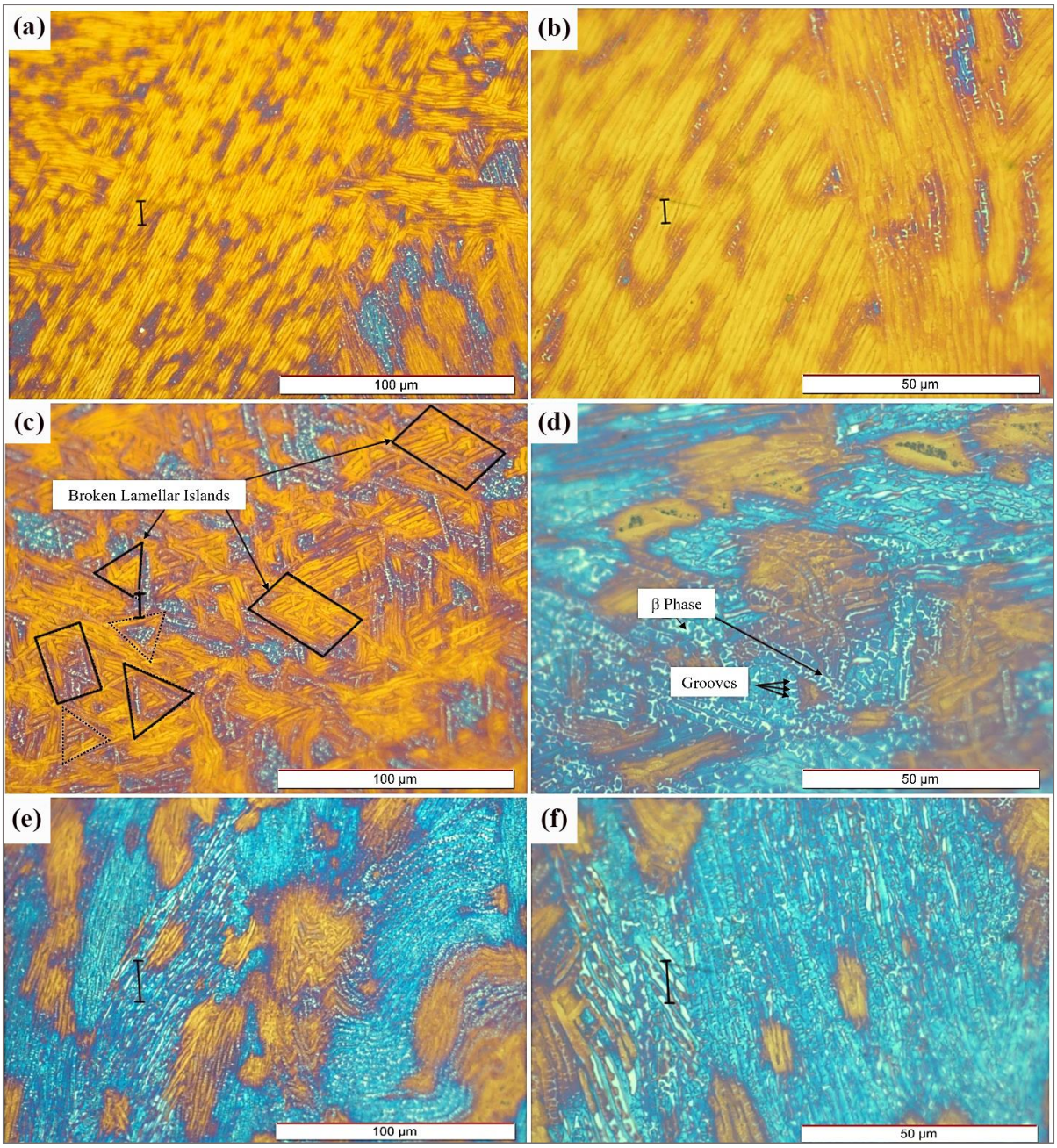

Fig. 11. The hot deformed microstructure of Ti-6Al-4V at 850 ˚C- 0.01 s^{-1} and different true strain of (a, b) 0.1, (c, d) 0.3 s^{-1}, and (e, f) 0.5 s^{-1}.

In geometric dynamic recrystallization, the original grains are flattened due to compressive deformation, and then boundary serrations are created. The serration impinges to each other, and the new grains are formed. The GDRX and lamellar kinking are known as the first fracture mechanism of lamellar microstructure in the Ti-6Al-4V alloy. In the unified globularization mechanism, including the boundary splitting, shearing mechanism, and termination migration, the deformation inhomogeneity created the sub-grain boundary with high dislocation density on the lamellar grains. This region acts as a channel for solute atom diffusion [37]. The elemental concentration gradient in the lamellar leads to the groove's formation in the microstructure (Fig. 11(d)). In the grooves, the α-phase becomes unstable and is replaced by the β-phase and then the α phase is separated from the lamellar grain.

4. Conclusion

The hot compression behavior of fully lamellar Ti-6Al-4V alloy was investigated at a temperature range of 700-1050 ˚C and strain rate range of 0.001-1 s^{-1}. The main conclusions can be summarized as follows:

(1) Based on true stress-strain curves, the dynamic recrystallization was a dominant softening mechanism at lower strain rates than 0.1 s^{-1}. On the other hand, the dynamic recovery mechanism was activated in the β-phase region and also the high strain rate deformation (1 s^{-1}) in the α-phase.

(2) Dynamic strain aging appeared as serrated effects on the stress-strain curve at the lowest strain rate at a deformation temperature of 800 ˚C.

(3) The activation energy values were calculated at about 630 kJ/mol and 293 kJ/mol for α and β-phase regions. By determining the power exponents in α phase (~ 6.5) and β phase (~3.7), the constitutive equations in these phases were derived.

(4) The globularization occurred during hot deformation in the temperature range of 850-900 ˚C. The formation of β-phase grooves within the α lamellar resulted in the division of lamellar into globularized grains. Microstructural evolution including α lamellar kinking and fragmentation and geometric dynamic recrystallization occurred below the globularization temperature.

Conflict of Interests

The authors state that they have no conflicts of interest to disclose.

Funding

The research was supported by Atomic Energy Organization of Iran.

5. References

[1] Ji, S. M., Jang, S. M., Lee, Y. S., Kwak, H. M., Choi, J. M., & Joun, M. S. (2022). Characterization of Ti-6Al-4V alloy in the temperature range of warm metal forming and fracture analysis of the warm capping process. *Journal of Materials Research and Technology*, *18*, 1590-1606. https://doi.org/10.1016/j.jmrt.2022.03.066

[2] Bignon, Q., Martin, F., Auzoux, Q., Miserque, F., Tabarant, M., Latu-Romain, L., & Wouters, Y. (2019). Oxide formation on titanium alloys in primary water of nuclear pressurised water reactor. *Corrosion Science*, *150*, 32-41. https://doi.org/10.1016/j.corsci.2019.01.020

[3] Leyens, C., & Peters, M. (Eds.). (2006). *Titanium and titanium alloys: fundamentals and applications*. Wiley-vch.

[4] Donachie, M. J. (2000). *Titanium: a technical guide*. ASM international.

[5] Gheshlaghi, H., Alimirzaloo, V., Shahbaz, M., & Amiri, A. (2022). Numerical study and optimization of the thermomechanical procedure in forging of two-phase Ti-6Al-4V Alloy for artificial hip joint implant. *Iranian Journal of Materials Forming*, *9*(3), 31-43. https://doi.org/10.22099/ijmf.2022.43334.1219

[6] Ishida, T., Wakai, E., Makimura, S., Casella, A. M., Edwards, D. J., PrabhakaranSenor., D. J., Ammigan, K., Bidhar, S., Hurh, P. G., Pellemoine, F., Densham, C. J., Fitton, M. D., Bennett, J. M., Kim, D., Simos, N., Hagiwara, M., Kawamura, N., Meigo, Sh., & Yonehara, K (2020). Tensile behavior of dual-phase titanium alloys under high-intensity proton beam exposure: Radiation-induced omega phase transformation in Ti-6Al-4V. *Journal of Nuclear Materials*, *541*, 152413. https://doi.org/10.1016/j.jnucmat.2020.152413

[7] Ishida, T., Wakai, E., Makimura, Sh., Hurh, P. G., Ammigan, K., Casella, A. M., Edwards, D. J., Senor, D. J., Densham, C. J., Fitton, M., Bennett, J., Kim, D., Simos, N., Calviani, M., & Torregrosa Martin, C

(2020). Radiation damage studies on titanium alloys as high intensity proton accelerator beam window materials. In *Proceedings of the 14th International Workshop on Spallation Materials Technology* (p. 041001). https://doi.org/10.7566/JPSCP.28.041001

[8] Chen, G., Ren, C., Qin, X., & Li, J. (2015). Temperature dependent work hardening in Ti–6Al–4V alloy over large temperature and strain rate ranges: Experiments and constitutive modeling. *Materials & Design*, *83*, 598-610. https://doi.org/10.1016/j.matdes.2015.06.048

[9] Wu, G. Q., Shi, C. L., Sha, W., Sha, A. X., & Jiang, H. R. (2013). Effect of microstructure on the fatigue properties of Ti–6Al–4V titanium alloys. *Materials & Design (1980-2015)*, *46*, 668-674. https://doi.org/10.1016/j.matdes.2012.10.059

[10] Lin, Y. C., Jiang, X. Y., Shuai, C. J., Zhao, C. Y., He, D. G., Chen, M. S., & Chen, C. (2018). Effects of initial microstructures on hot tensile deformation behaviors and fracture characteristics of Ti-6Al-4V alloy. *Materials Science and Engineering: A*, *711*, 293-302. https://doi.org/10.1016/j.msea.2017.11.044

[11] Jia, M. T., Zhang, D. L., Gabbitas, B., Liang, J. M., & Kong, C. (2015). A novel Ti–6Al–4V alloy microstructure with very high strength and good ductility. *Scripta Materialia*, *107*, 10-13. https://doi.org/10.1016/j.scriptamat.2015.05.008

[12] Jiang, F., Fei, L., Jiang, H., Zhang, Y., Feng, Z., & Zhao, S. (2023). Constitutive model research on the hot deformation behavior of Ti6Al4V alloy under wide temperatures. *Journal of Materials Research and Technology*, *23*, 1062-1074. https://doi.org/10.1016/j.jmrt.2023.01.021

[13] Bodunrin, M. O., Chown, L. H., van der Merwe, J. W., & Alaneme, K. K. (2019). Hot working of Ti-6Al-4V with a complex initial microstructure. *International Journal of Material Forming*, *12*, 857-874. https://doi.org/10.1007/s12289-018-1457-9

[14] Huang, X., Zang, Y., & Guan, B. (2021). Constitutive models and microstructure evolution of Ti-6Al-4V alloy during the hot compressive process. *Materials Research Express*, *8*(1), 016534. https://doi.org/10.1088/2053-1591/abdaf0

[15] Jha, J. S., Tewari, A., Mishra, S., & Toppo, S. (2017). Constitutive relations for Ti-6Al-4V hot working. *Procedia Engineering*, *173*, 755-762. https://doi.org/10.1016/j.proeng.2016.12.089

[16] Bruschi, S., Poggio, S., Quadrini, F., & Tata, M. E. (2004). Workability of Ti–6Al–4V alloy at high temperatures and strain rates. *Materials Letters*, *58*(27-28), 3622-3629. https://doi.org/10.1016/j.matlet.2004.06.058

[17] Momeni, A., & Abbasi, S. M. (2010). Effect of hot working on flow behavior of Ti–6Al–4V alloy in single phase and two phase regions. *Materials & Design*, *31*(8), 3599-3604. https://doi.org/10.1016/j.matdes.2010.01.060

[18] Hu, M., Dong, L., Zhang, Z., Lei, X., Yang, R., & Sha, Y. (2018). Correction of flow curves and constitutive modelling of a Ti-6Al-4V alloy. *Metals*, *8*(4), 256. https://doi.org/10.3390/met8040256

[19] Wu, Y., Liu, H., Xu, J., Zhang, Z., & Xue, Y. (2020). Constitutive equations and processing map for hot deformation of a Ti-6Al-4V alloy prepared with spark-plasma sintering. *Materials & Technologies/Materiali in Tehnologije*, *54*(1). https://doi.org/10.17222/mit.2019.087

[20] Jha, J. S., Toppo, S. P., Singh, R., Tewari, A., & Mishra, S. K. (2019). Flow stress constitutive relationship between lamellar and equiaxed microstructure during hot deformation of Ti-6Al-4V. *Journal of Materials Processing Technology*, *270*, 216-227. https://doi.org/10.1016/j.jmatprotec.2019.02.030

[21] Lin, Y. C., Zhao, C. Y., Chen, M. S., & Chen, D. D. (2016). A novel constitutive model for hot deformation behaviors of Ti–6Al–4V alloy based on probabilistic method. *Applied Physics A*, *122*, 1-9. https://doi.org/10.1007/s00339-016-0248-8

[22] Lin, Y. C., Wu, Q., Pang, G. D., Jiang, X. Y., & He, D. G. (2020). Hot tensile deformation mechanism and dynamic softening behavior of Ti–6Al–4V alloy with thick lamellar microstructures. *Advanced Engineering Materials*, *22* (3), 1901193. https://doi.org/10.1002/adem.201901193

[23] Dhanya, M. S., Anoop, S., Manwatkar, S. K., Kumar, R. R., Gupta, R. K., & Narayana Murty, S. V. S. (2024). Hot workability and microstructure control of Ti6Al4V alloy. *Journal of Materials Engineering and Performance*, 1-17. https://doi.org/10.1007/s11665-024-09228-6

[24] Ebrahimi, R., & Najafizadeh, A. (2004). A new method for evaluation of friction in bulk metal forming. *Journal of Materials Processing Technology*, *152*(2), 136-143. https://doi.org/10.1016/j.jmatprotec.2004.03.029

[25] Gostariani, R., & Asadi Asadabad, M. (2023). Studying the hot deformation behavior of Zr-1Nb alloy using processing map and kinetic analysis. *Journal of Materials Engineering and Performance*, *32*(5), 2151-2164. https://doi.org/10.1007/s11665-022-07267-5

[26] Sellars, C. M., & McTegart, W. J. (1966). On the mechanism of hot deformation. *Acta Metallurgica*, *14*(9), 1136-1138. https://doi.org/10.1016/0001-6160(66)90207-0

[27] Zener, C., & Hollomon, J. H. (1944). Effect of strain rate upon plastic flow of steel. *Journal of Applied Physics*, *15*(1), 22-32. https://doi.org/10.1063/1.1707363

[28] Lin, Y. C., & Chen, X. M. (2011). A critical review of experimental results and constitutive descriptions for metals and alloys in hot working. *Materials & Design*, *32*(4), 1733-1759.

https://doi.org/10.1016/j.matdes.2010.11.048

[29] Kazim, S. M., Prasad, K., & Chakraborty, P. (2023). Analysis of dynamic strain aging in titanium alloys using CPFEM. *Materials Today: Proceedings*. https://doi.org/10.1016/j.matpr.2023.07.268

[30] Prasad, K., & Varma, V. K. (2008). Serrated flow behavior in a near alpha titanium alloy IMI 834. *Materials Science and Engineering: A*, *486*(1-2), 158-166. https://doi.org/10.1016/j.msea.2007.09.020

[31] Zhang, Z. X., Qu, S. J., Feng, A. H., Shen, J., & Chen, D. L. (2017). Hot deformation behavior of Ti-6Al-4V alloy: Effect of initial microstructure. *Journal of Alloys and Compounds*, *718*, 170-181. https://doi.org/10.1016/j.jallcom.2017.05.097

[32] Jonas, J. J., Sellars, C. M., & Tegart, W. M. (1969). Strength and structure under hot-working conditions. *Metallurgical Reviews*, *14*(1), 1-24. https://doi.org/10.1179/mtlr.1969.14.1.1

[33] Ning, Y. Q., Xie, B. C., Liang, H. Q., Li, H., Yang, X. M., & Guo, H. Z. (2015). Dynamic softening behavior of TC18 titanium alloy during hot deformation. *Materials & Design*, *71*, 68-77. https://doi.org/10.1016/j.matdes.2015.01.009

[34] Kim, J. H., Semiatin, S. L., Lee, Y. H., & Lee, C. S. (2011). A self-consistent approach for modeling the flow behavior of the alpha and beta phases in Ti-6Al-4V. *Metallurgical and Materials Transactions A*, *42*, 1805-1814. https://doi.org/10.1007/s11661-010-0567-x

[35] Guo, B., & Jonas, J. J. (2021). Dynamic transformation during the high temperature deformation of titanium alloys. *Journal of Alloys and Compounds*, *884*, 161179. https://doi.org/10.1016/j.jallcom.2021.161179

[36] Guo, B., Semiatin, S. L., & Jonas, J. J. (2019). Dynamic transformation during the high temperature deformation of two-phase titanium alloys. *Materials Science and Engineering: A*, *761*, 138047. https://doi.org/10.1016/j.msea.2019.138047

[37] Zhang, J., Li, H., & Zhan, M. (2020). Review on globularization of titanium alloy with lamellar colony. *Manufacturing Review*, *7*, 18. https://doi.org/10.1051/mfreview/2020015

[38] Ezatpour, H. R., Ebrahimi, G. R., & Zarghani, F. (2024). Effect of processing parameters on the morphology of α-phase in Ti-6Al-4V alloy during the two-step hot deformation. *Iranian Journal of Materials Forming*, *10*(3), 54-62. https://doi.org/ 10.22099/ijmf.2024.49049.1277